Received: 6 July 2021 | Revised: 29 September 2021 | Accepted: 12 October 2021
DOI: 10.1111/jre.12946

ORIGINAL ARTICLE

Journal of PERIODONTAL RESEARCH WILEY

Functional Adaptation of LPS-affected Dentoalveolar Fibrous Joints in Rats

Bo Wang[1] | **Putu Ustriyana**[1] | **Caleb. S. Tam**[1,2] | **Jeremy. D. Lin**[1] | **Sudarshan Srirangapatanam**[1] | **Yvonne Kapila**[3] | **Mark I. Ryder**[3] | **Samuel Webb**[4] | **Youngho Seo**[2] | **Sunita. P. Ho**[1,5]

[1]Division of Preclinical Education, Biomaterials & Engineering, Department of Preventive and Restorative Dental Sciences, School of Dentistry, University of California, San Francisco, US

[2]Department of Radiology and Biomedical Imaging, School of Medicine, University of California, San Francisco, US

[3]Division of Periodontology, Department of Orofacial Sciences, School of Dentistry, University of California, San Francisco, US

[4]Stanford Synchrotron Radiation Lightsource, SLAC National Accelerator Laboratory, Menlo Park, US

[5]Department of Urology, School of Medicine, University of California, San Francisco, US

Correspondence
Sunita P Ho, Division of Preclinical Education, Biomaterials & Engineering, Department of Preventive and Restorative Dental Sciences, 513 Parnassus Avenue, Room HSW813, University of California, San Francisco, CA 94143-0758
Email: sunita.ho@ucsf.edu

Funding information
National Institutes of Health, NIDCR R01 DE022032 (SPH) and NIDCR R21 DE027138 (SPH)

Abstract

Introduction: The functional interplay between cementum of the root and alveolar bone of the socket is tuned by a uniquely positioned 70–80 μm wide fibrous and lubricious ligament in a dentoalveolar joint (DAJ). In this study, structural and biomechanical properties of the DAJ, periodontal ligament space (PDL-space also known as the joint space), alveolar bone of the socket, and cementum of the tooth root that govern the biomechanics of a lipopolysaccharide (LPS)-affected DAJ were mapped both in space and time.

Methods: The hemi-maxillae from 20 rats (4 control at 6 weeks of age, 4 control and 4 LPS-affected at 12 weeks of age, 4 control and 4 LPS-affected at 16 weeks of age) were investigated using a hybrid technique; micro-X-ray computed tomography (5 μm resolution) in combination with biomechanical testing *in situ*. Temporal variations in bone and cementum volume fractions were evaluated. Trends in mineral apposition rates (MAR) in additional six Sprague Dawley rats (3 controls, 3 LPS-affected) were revealed by transforming spatial fluorochrome signals to functional growth rates (linearity factor - RW) of bone, dentin, and cementum using a fast Fourier transform on fluorochrome signals from 100-μm hemi-maxillae sections.

Results: An overall change in LPS-affected DAJ biomechanics (a 2.5–4.5X increase in tooth displacement and 2X tooth rotation at 6 weeks, no increase in displacement and a 7X increase in rotation at 12 weeks; 27% increase in bone effective strain at 6 weeks and 11% at 12 weeks relative to control) was associated with structural changes in the coronal regions of the DAJ (15% increase in PDL-space from 0 to 6 weeks but only 5% from 6 to 12 weeks compared to control). A significant increase ($p < 0.05$) in PDL-space between ligated and age-matched control was observed. The bone fraction of ligated at 12 weeks was significantly lower than its age-matched control, and no significant differences

Abbreviations: a.u, arbitrary unit; AUC, area under the curve; BF, bone fraction; C, control; CF, cementum fraction; CR-B, crestal bone; DA, distal aspect; DAJ, dentoalveolar joint; D-CR, distal crestal location; DOF, degrees of freedom; DR, distal root; DVC, digital volume correlation; FFT, fast Fourier transform; FWHM, full-width at half-maximum; ID, inter-dental; IR, interradicular; L, ligated; LPS, lipopolysaccharide; MA, mesial aspect; MAR, mineral apposition rate – see supplemental information for definition and calculation; M-CR, mesial crestal location; MR, mesial root; PDL, periodontal ligament; R1-R4, Roots 1–4; RD, relative duration, or the duration of occurrence of a mineral apposition event; ROI, region of interest; RW, relative weight – see supplemental information for definition and calculation; wk, week; XCT, X-ray computed tomography.

Bo Wang, Putu Ustriyana and C.S. Tam equal contribution and are first authors.

($p > 0.05$) between groups were observed at 6 weeks. Cementum in the apical regions grew faster but nonlinearly (11% and 20% increase in cementum fraction (CF) at 6 and 12 weeks) compared to control. Alveolar bone revealed site-specific nonlinear growth with an overall increase in MAR (108.5 μm/week to 126.7 μm/week after LPS treatment) compared to dentin (28.3 μm/week in control vs. 26.1 μm/week in LPS-affected) and cementum (126.5 μm/week in control vs. 119.9 μm/week in LPS-affected). A significant increase in CF ($p < 0.05$) in ligated specimens was observed at 6 weeks of age.

Conclusions: Anatomy-specific responses of cementum and bone to the mechano-chemo stimuli, and their collective temporal contribution to observed changes in PDL-space were perpetuated by altered tooth movement. Data highlight the "resilience" of DAJ function through the predominance of nonlinear growth response of cementum, changes in PDL-space, and bone architecture. Despite the significant differences in bone and cementum architectures, data provided insights into the reactionary effects of cementum as a built-in compensatory mechanism to reestablish functional competence of the DAJ. The spatial shifts in architectures of alveolar bone and cementum, and consequently ligament space, highlight adaptations farther away from the site of insult, which also is another novel insight from this study. These adaptations when correlated within the context of joint function (biomechanics) illustrate that they are indeed necessary to sustain DAJ function albeit being pathological.

KEYWORDS

Biomechanics, cementum, dentoalveolar joint, endotoxin, fluorochrome, histomorphometrics, morphometrics, periodontal ligament (PDL), periodontal tissues/periodontium

1 | INTRODUCTION

Skeletal, oral, and craniofacial joints are routinely insulted in multiple ways. Periodontal tissues that constitute a dentoalveolar joint (DAJ) adapt, and these adaptations are dependent on the magnitude, frequency, and duration of an insult (1-3). Insults often present themselves as mechanical and/or microbial loads. Resulting tissue adaptations are routinely documented only at the site of insult (4,5). No information exists on tissue adaptations in regions farther away from the insult, as no apparent insult or its effect in these regions is presumed.

Periodontitis is a chronic inflammatory disease mediated by a microbial dysbiosis (an insult) that has distinct acute patterns including gingival tissue inflammation and chronic alveolar bone (attachment) loss (4). Anatomy-specific crestal and interradicular bone loss in the periodontal complex is routinely documented in patients with periodontitis. These physical measurements are used as diagnostic markers to estimate disease severity (4-6). Diagnostic measures to date are localized to sites of insult, mainly the coronal portion of the periodontal complex. In the presence of such a microbe-induced chronic disease, we hypothesized that prolonged physical (chewing forces) and chemical (endotoxin) cues will prompt tissue chemo- and mechano-adaptation (7) and exacerbate joint-level biomechanics.

The tooth within the alveolar socket enveloped with the gingival tissue is a single joint (8); the tooth is attached to the alveolar bone with a fibrous innervated and vascularized periodontal ligament (PDL). The six degrees of freedom (DOFs) allow the tooth to translate (in three directions, X, Y, and Z) and rotate (about X, Y, and Z) within the alveolar socket but are limited to the PDL-space (70 μm in rats) specifically when mechanical loads are within physiological limits. The approach taken in this study will investigate the hypothesis that prolonged chewing function of a DAJ affected by lipopolysaccharide (LPS), a bacterial endotoxin and virulence factor (9,10) used as a chemical cue, can exacerbate temporal adaptation of the periodontal tissues, in particular, cementum, dentin, and the alveolar bone.

The hypothesis was investigated using Sprague Dawley rats. The coupled effects of LPS insult (chemical cue) in the presence of chewing function (mechanical cue) on the DAJs of rats will be illustrated as shifts in spatiotemporal physical properties of periodontal tissues including cementum and bone. Shifts in translational and rotational components of the tooth relative to the alveolar bone will be visualized using a hybrid functional imaging method (11). Multiscale biomechanical testing *in situ* of the DAJ and dynamic histomorphometry will (1) highlight the effectiveness of anatomy-specific shifts in tensile and compressive strain profiles in alveolar bone; (2) provide insights into the observed acute and chronic shifts in physical properties of the LPS-affected periodontal tissues; and (3) reveal that these anatomy-specific adaptations are axiomatic to meet the overall functional demands on an LPS-insulted DAJ. The temporal anatomy-specific adaptations in dentin, cementum, and alveolar bone marked by fluorochrome will illustrate that (4) the chronic yet adaptive disposition of these tissues to mechano-chemo stimuli is perpetuated by changes in joint space.

2 | MATERIALS AND METHODS

2.1 | Animal model and LPS-affected periodontal complex

All animal experiments were approved by the Institutional Animal Care and Use Committee (IACUC), University of California, San Francisco (UCSF) (AN083692 and AN080608-02). LPS-soaked (1mg of lipopolysaccharide (LPS) from *Escherichia coli* serotype 055:B5 (Sigma-Aldrich, St. Louis, MO, USA) per 1mL of 1x Tris buffer) 4–0 silk ligatures were tied around the second molar of rats at 6 weeks of age (12-14). Ligatures were placed between the first and second molars and the second and third molars of both maxillae as described in our previous study (12). Molars were religated every 2–3 days to ensure retention. Control rats (N = 6 per time point) were flossed every 2–3 days with 4–0 silk ligatures without LPS. 20 rats (12 control, 8 LPS-affected) were euthanized after 6 and 12 weeks of ligation. Maxillae were harvested and hemisected. Right hemi-maxillae were stored in 70% ethanol for micro-XCT analysis. These maxillae were used for macrostructural analyses via micro-X-ray computed tomography (micro-XCT) followed by one hemi-maxilla from each group for DAJ biomechanical testing *in situ*. Additional six male Sprague Dawley rats (3 control, 3 LPS-affected) were used for dynamic histomorphometry and mineral apposition rate (MAR) analyses. All experiments *in vivo* were reported following the ARRIVE 2.0 checklist.

Fluorochrome injection and specimen preparation: Each of the 3 control and 3 LPS-affected rats were given 10 alternating intraperitoneal injections of 0.01 mg/μL tetracycline hydrochloride (HCl) and alizarin red dyes (Sigma-Aldrich) over 11 weeks (15-17). The injections were initiated at 6 weeks of age and were repeated once weekly for the first 6 weeks and twice for every 1.5 weeks.

Rats were euthanized after 12 weeks (rat age: 18 weeks) of endotoxin treatment, and the hemi-maxillae were dissected. Each hemi-maxilla was reduced to a 100 μm thick slice. Slices were mounted on glass microscope slides with coverslips for optical and X-ray imaging.

2.2 | Micro-XCT and biomechanical testing *in situ* of the DAJ

The second maxillary DAJs were imaged using micro-XCT at 4X magnification. Specimens immersed in 70% ethanol with the second molar centered in the field of view were scanned. Tomograms were reconstructed (XMReconstructor v8.1.6599, Xradia Inc., Pleasanton, CA, USA), and post analyses using Avizo (Avizo 2019.4, FEI Visualization Sciences Group, Burlington, MA, USA) were performed on digital volumes of the hemi-maxillae.

Physical properties of periodontal tissues: The PDL-space, bone fraction (BF), and cementum fraction (CF) surrounding the second maxillary molar for each specimen were estimated from the local regions of interest (ROIs) at the mesial and distal locations of the periodontal complex (Figure A.1). Statistical differences between groups were evaluated using Student's t-test with a 95% confidence interval.

Biomechanical testing in situ of the DAJ: The second maxillary molars of rats from experimental weeks 6 and 12 were scanned at no load in the micro-XCT. Specimens were loaded to 15 N followed by another scan. Displacements and rotations of the second molar within the bony socket described in our previous studies (18) were evaluated to determine the shifts in DOFs of the tooth. In brief, the DOF were measured by comparing the relative position (displacements and rotations about the X, Y, and Z axes) of the tooth within the socket at no load to when it is loaded.

Digital volume correlation to strain profiles in bone: Full-field maximum (tensile) and minimum (compressive) principal strains followed by the effective (volumetric) strain within the alveolar bone were evaluated (19,20) using DVC software (Appendix Material).

2.3 | Optical imaging of fluorochrome-stained bone, dentin, and cementum

Fluorescence images (Nikon 6D Ti-E conventional wide-field microscope) using mCherry epifluorescence to visualize alizarin red labels and sapphire epifluorescence to visualize tetracycline HCl labels were captured. Raw images were processed using Fiji (17). Images were stitched to generate a montage (Figure A.2).

Dynamic histomorphometry using fluorochrome signals: MARs in mineralized tissues were evaluated from the fluorochrome images. A custom-built fast Fourier transform (FFT) protocol was developed to estimate the rate of mineral apposition. After a series of signal processing steps, fluorochrome signals were analyzed to obtain values of MAR and RW (Figures A.2-5).

X-ray radiographs of fluorochrome sections: X-ray radiographs of each hemi-maxilla were taken at specifications comparable to that of fluorochrome images. Large-scale images of entire specimens were taken using the XM mosaic function in absorption mode at 20X magnification. For every fluorochrome measurement, an equivalent micro-XCT box plot was ascertained (Figures A.3B). Signals produced from micro-XCT images were assessed by the sign/slope of their intensity gradients across the length of each ROI. The final vector of higher to lower mineral density was taken to represent the overall direction of mineral apposition.

3 | RESULTS

The workflow (Figure 1) is organized within the context of the central hypothesis (Figure 1B) that prolonged chewing in the presence

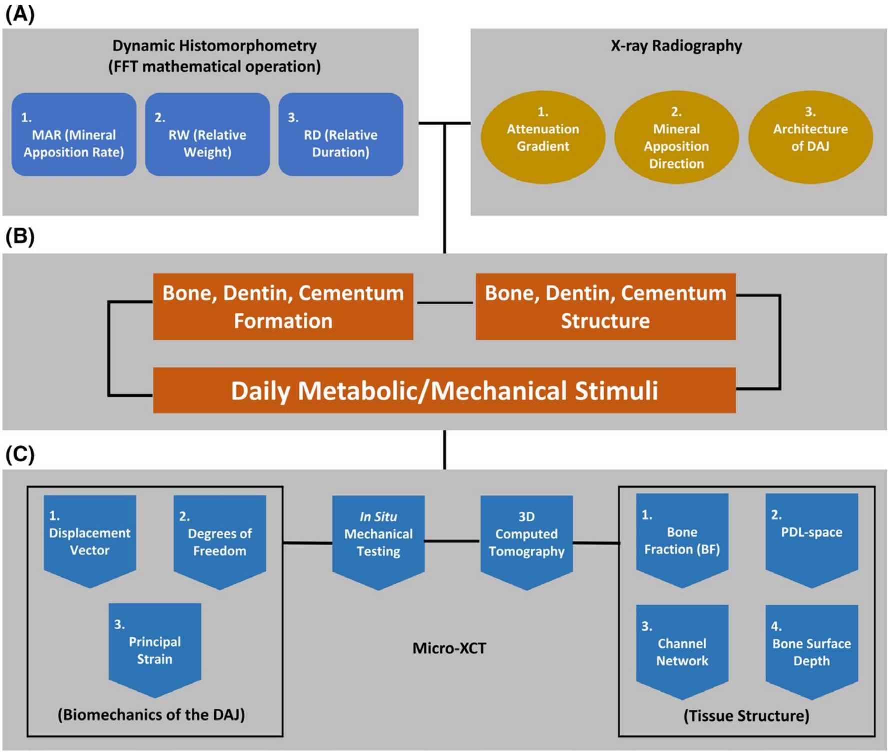

FIGURE 1 Methodology and measured outcomes of an LPS-affected dentoalveolar joint (DAJ). (A) Methodology, (B) objective, and (C) markers as outcome measures of shifts in DAJ biomechanics and resulting mechano-chemo adaptation of bone, dentin, and cementum within an LPS-affected yet functionally active DAJ are shown

of LPS endotoxin will exacerbate tissue adaptation. The closed loop represents that the changes in tissue-level physical parameters will affect joint biomechanics, and that the continuous crosstalk between tissue characteristics and joint function will occur in perpetuity. Output parameters from dynamic histomorphometry (MAR and relative weight (RW)) and correlative radiography (intensity gradients) will represent mineralized tissue growth rate, while final output parameters including the spatiotemporal shifts in PDL-space and bone and cementum fractions will be highlighted within the context of joint biomechanics (displacement vectors, DOFs, and principal/effective strains within bone) (Figure 1).

3.1 | Joint biomechanics and physical properties of periodontal tissues

Tooth translation and rotation in LPS-affected bony socket: Controlled biomechanical testing of the second molar (15 N of force) illustrated a 4.5X increase in the lingual and 2.5X increase in apical directions in tooth displacement at 6 weeks (Figure 2A). No differences in translation between control and LPS-affected specimens were observed at 12 weeks, except for the increase in degrees of rotation (2X at 6 weeks and 7X at 12 weeks).

Changes in the space between the tooth and bony socket: Increased PDL-spaces at the coronal and apical aspects of the periodontal complex resulting in an increased joint space in an LPS-affected DAJ compared to the control were observed (Figure 2B and Figure A.6). The joint space of the LPS-affected specimens returned to baseline values within 12 weeks. The temporal variations of joint space differed between control and LPS-affected specimens. On average, the joint space in the control group decreased from 0 to 6 weeks and remained relatively stable from 6 to 12 weeks. In contrast, the average joint space in the LPS-affected group significantly increased from 0 to 6 weeks but decreased from 6 to 12 weeks (Figure 2B). Statistically, no significant differences in PDL-spaces of controls at different ages were observed (Figure 2B3). However, a significant increase in PDL-space of ligated compared to its age-matched control was observed (Figure 2B3).

Compression and tension profiles in bone volumes: The overall tensile, compressive, and effective strains decreased from 6 weeks to 12 weeks in both groups. Higher strains were observed in LPS-affected group compared to control at both time points (Figure 2C). Effective strains in coronal, apical, and interradicular regions of LPS-affected alveolar bone were higher compared to that in the control group at both 6 and 12 weeks (Figure 2C, red arrows in Figure 2C2, Figures A.7 and A.8). Higher effective (compressive) strain in alveolar bone was associated with larger joint space in both control and LPS-affected groups (Figure 2C). The alveolar bone in 6-week rats illustrated relatively lower compressive strain compared to 12-week rats in LPS-affected alveolar bone with increasing joint space (black arrows, Figure 2D).

Changes in bone and cementum volumes: Bone fraction (BF) values in the control group were relatively higher than the LPS-affected group at 6 and 12 weeks (Figure 3A1 and 3B1). The decrease in BF values from 0 to 12 weeks in the LPS-affected group compared to control was apparent at the coronal one-third (mesial roots) and interradicular regions (Figure 3B1 and Figure A.9). Overall, the increase in BF in the control group was higher from 0 to 6 weeks than that from 6 to 12 weeks. BF in the LPS-affected group increased from 0 to 6 weeks but remained stable from 6 to 12 weeks (Figure 3C1). Maxillary bone fractions of

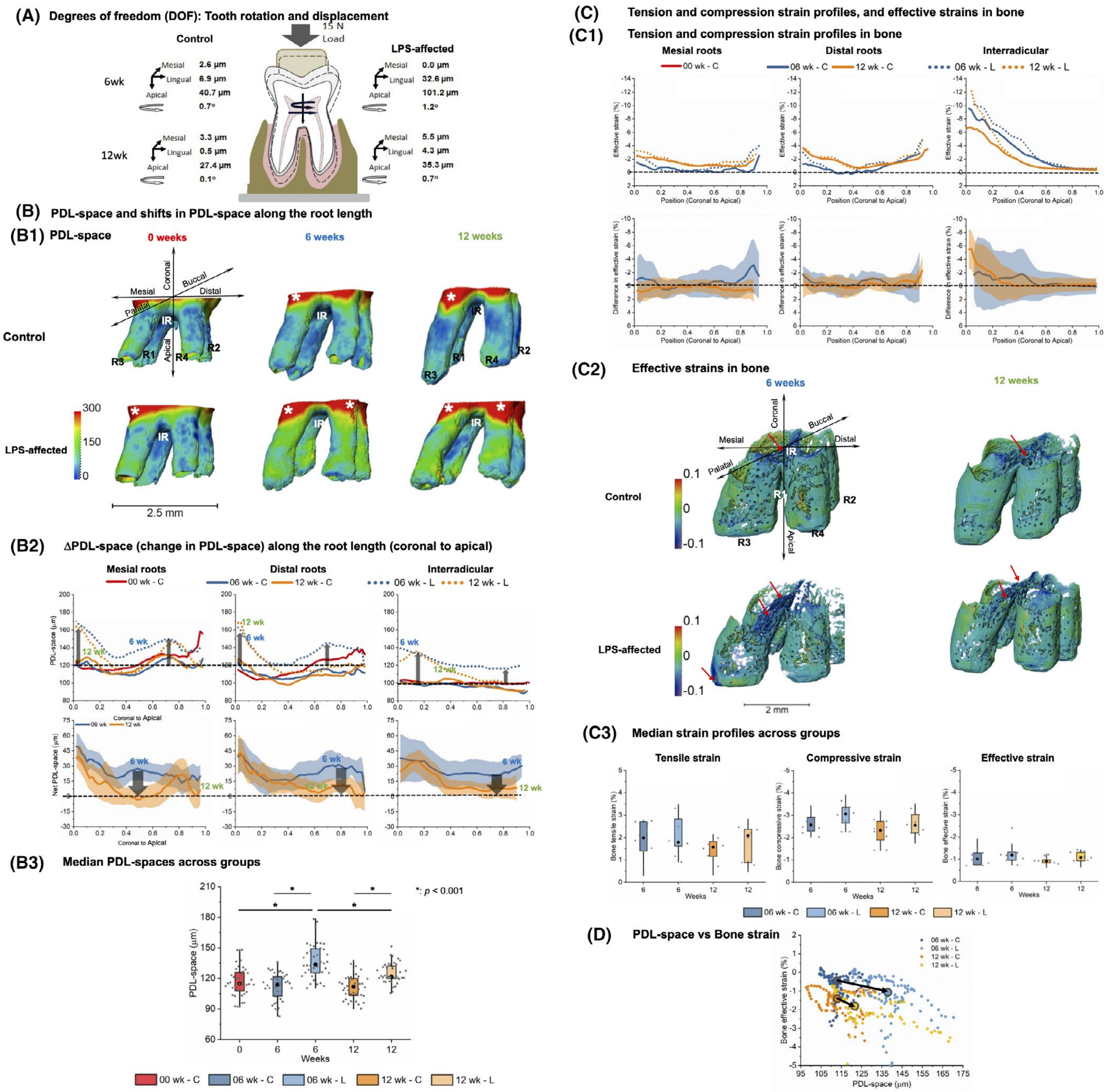

FIGURE 2 Sustained chewing using an LPS-affected DAJ at 6 weeks indicated decreased tooth movement at 12 weeks despite coronal bone loss. Higher compressive strains in LPS-affected alveolar bone with increasing PDL-space were observed. (A) Schematic illustrates LPS-affected DAJ with a net increase in displacement and rotation at 6 weeks but a decrease at 12 weeks. (B) Spatial maps of PDL-spaces from control and LPS-affected groups at 0, 6, and 12 weeks illustrate narrowed (light to dark blue shades) and widened (green, yellow, and red shades) spaces (B1). See Figure A.6 for anatomy-specific PDL-space. PDL-space and its difference between LPS-affected and control groups (ΔPDL-space) along the root length (coronal-apical) are specific to anatomical locations (mesial, distal, and interradicular regions). 95% confidence intervals for average ΔPDL-spaces within mesial, distal, and interradicular regions from coronal to apical locations of respective roots are represented as light blue (6 weeks) and orange (12 weeks) (B2). Box plots illustrate spread of data and median PDL-spaces in control and LPS-affected DAJs at 0, 6, and 12 weeks (B3). (C) Effective strain and its difference between LPS-affected and control groups (Δbone effective strain) along the root length (coronal-apical) indicated anatomy-specific trends. 95% confidence interval for average Δbone effective strain within mesial, distal, and interradicular regions is represented as light blue and orange zones (C1). Maps of effective strains within alveolar bones in LPS-affected groups at 6 and 12 weeks are shown (C2). Box plots of tensile, compressive, and effective strains within control and LPS-affected groups at 6 and 12 weeks are shown (C3). (D) Correlative plots between PDL-space and bone strain indicated higher compressive strain within alveolar bone for an increase in PDL-space (black arrows mark the trend and direction). This trend was not age-specific, although LPS-affected bone in 12 weeks demonstrated higher compressive strain compared to that in 6 weeks. R1–R4: Roots 1 through 4; IR: interradicular

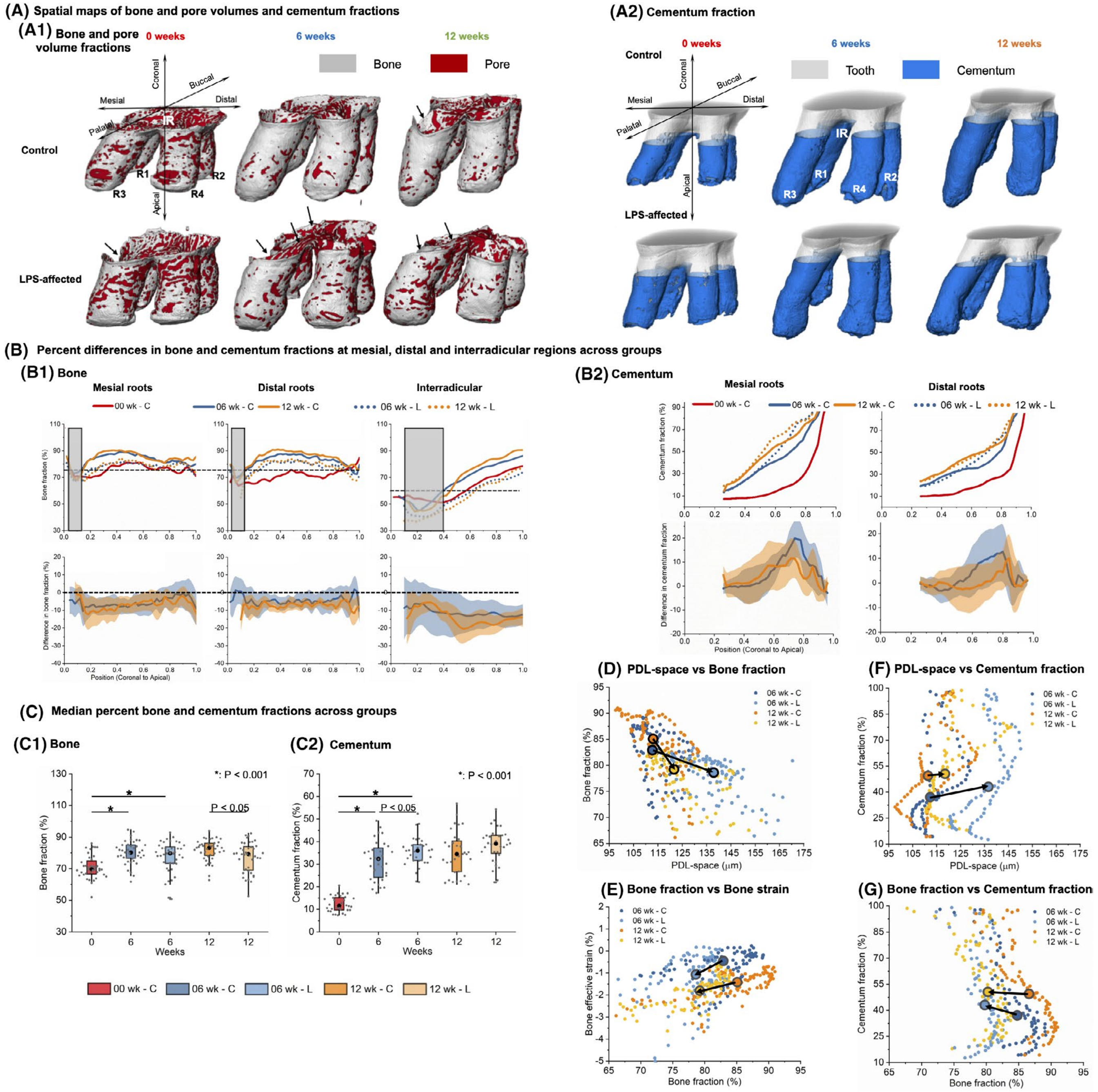

FIGURE 3 Alveolar bone fraction (BF) was lower in the coronal and interradicular regions, and cementum fraction (CF) was higher in apical regions of an LPS-affected DAJ. A nonlinear increase in CF in the distal roots compared to a linear increase in mesial roots of LPS-affected DAJs at both 6 and 12 weeks was observed. (A) Rendered bone (gray) and pore (red) volumes (A1), and CF (A2) in control and LPS-affected groups at 0, 6, and 12 weeks after ligation are shown. (B) Differences in BF (B1) and CF (B2) between LPS-affected and control groups along the root length (coronal-apical) illustrate variation along the root-length with significant losses in anatomy-specific regions. 95% confidence intervals for average difference in BF at the mesial, distal, and interradicular regions are shown. (C) Box plots show BF (C1) and CF (C2) in control and LPS-affected groups at 0, 6, and 12 weeks. Correlative plots illustrate (D) an increase in PDL-space for a decrease in BF; (e) for a percent decrease in BF, an increase in compressive strain in bone (black arrows mark the trend and direction) was observed; (F) CF increase for an increase in PDL-space, and (G) for a decrease in BF. R1–R4: Roots 1 through 4; IR: interradicular. See Figures A.7–9 for more information

controls increased significantly with age ($p < 0.05$). The bone fraction of a ligated at 12 weeks, however, was significantly lower ($p < 0.05$) than its age-matched control (Figure 3C1), and no significant difference ($p > 0.05$) between ligated and control was observed at 6 weeks. The trends of BF in both control and LPS-affected groups were inversely proportional to the PDL-spaces (Figure 3D). LPS-affected specimens were associated with relatively lower BF despite having a similar bone effective strain value relative to the control group (Figure 3E).

Coronal compared to apical CF was lower in both control and LPS-affected groups and was as expected (Figures 3A2 and 3B2). A significant increase in CF from 0 to 12 weeks in the apical locations of the LPS-affected group relative to control was observed (Figure 3C2). An apparent change in CF from 0 to 6 weeks than that from 6 to 12 weeks was observed in both the control and LPS-affected groups. The increasing trend in CF, however, was greater in the LPS-affected group compared to the control group from 0 to 12 weeks (Figure 3C2) and was observed with increasing PDL-space (Figure 3F). The CF in the LPS-affected group was larger than age-matched controls at 6 and 12 weeks (Figure 3C2) and contrasted with respective BF (Figure 3G). While the age-related trends for bone and cementum were the same, a significant increase ($p < 0.05$) in CF of 6-week ligated specimens was observed (Figure 3C2).

3.2 | Mineral apposition rates in bone, cementum, and dentin of the maxillary complex

Correlative spatiotemporal maps of X-ray intensities and fluorochrome patterns: The organized strata/lamellae in the control specimen contrasted with the unorganized patterns in bone (B), dentin (D), and cementum (C) of the LPS-affected periodontal complex (white arrows, Figures 4A and 4B). Correlative microscopy revealed significant mineral apposition in the coronal-apical regions of the alveolar bone from both groups (asterisk, Figures 4A and 4B) and mineral apposition in mesial-distal (triangle) direction of the alveolar bone in control group only (Figures 4A and 4E, X-ray maps for LPS-affected are not shown because no fluorochrome labels were observed in mesial-distal directions, see Figure 4B). Coronal-apical apposition was significant through fluorochrome labeling (Figure 4B) in the LPS-affected alveolar bone. Mesial-distal apposition in dentin (Figure 4F) and coronal-apical apposition in cementum (Figure 4G) were observed by correlating X-ray intensity with fluorochrome patterns.

Mineral apposition rates (MAR) in bone, cementum, and dentin: In both control and LPS-affected groups, MAR values varied widely in bone and cementum, but not in dentin. Variations in MAR values of cementum were relatively higher in the LPS-affected compared to the control specimens (larger spread of MAR data for cementum compared with bone and dentin, Figures 4H and 4I). An RW of 1 indicates a linear mineral apposition. Dentin in both control and LPS-specimens grew linearly (single frequency) compared to nonlinear site-specific growths observed in bone and cementum (3 frequencies for bone and 4 frequencies for cementum in LPS-affected compared to control) (Figure 4H, 4I and Figure A.10).

4 | DISCUSSION

The three fundamental physical features and structural components that affect DAJ function are (1) the joint space (PDL-space) between the tooth and the bony socket, (2) the alveolar bony socket (shape and mechanical properties), and (3) the tooth volume (cementum and dentin volumes). The observed changes in joint spaces and tissue volumes from a structural engineering perspective are in response to the tooth movement in the bony socket. The varied tooth movement in the bony socket can shift the physicochemical properties of the periodontal tissues, including bone, both in space (coronal, apical, mesial, and distal) and time (acute and chronic). The objective of this study was to evaluate the functional status of a DAJ and correlate the measured freedom of tooth movement to the shifts in physicochemical properties of the periodontal tissues in the presence of endotoxin (pathological insult a metabolic stimuli/chemical cue) and chewing forces (physiological function/mechanical cue) (Figure 1). Correlative plots between PDL-spaces and physicochemical properties of bone and cementum along the root length and over time revealed plausible adaptive processes at sites farther away from the site of insult.

The functional status of the periodontal complex was quantitated by mapping a regain in LPS-affected tooth movement which was similar to controls. The decreased tooth translation indicated a recovery of the functional status of the DAJ at 18 weeks despite the sustained effect of LPS endotoxin for 12 weeks. This recovery in functional status of the DAJ over time could result from the adaptive nature of chemo- and mechano-sensitive periodontal tissues (Figure 2A). LPS is an endotoxin (9,10) and is known to promote periodontal tissue breakdown (21,22). The temporal contrast in functional status of the periodontal complex (12 weeks vs. 18 weeks) initially revealed an acute effect of the endotoxin for 6 weeks, a metabolic stimulus that was dominant over the mechanical stimulus, namely, chewing forces. The sustained chewing for an additional 6 weeks on an already compromised 12-week-old periodontal tissues revealed a chronic yet seemingly favorable effect of chewing forces (regain in DOFs despite increased rotation, Figure 2A).

During the first 6 weeks, the increased tooth movement (Figures 2A and 2B) correlated with increased compressive strain in the interradicular and apical regions of the LPS-affected alveolar bone (Figure 2C). This effect of endotoxin-induced hyperfunction was further highlighted as an increase in effective strain (compressive) in regions farther away from the primary site of insult. The change in strain profiles in bone also revealed the effect of physical property changes in tissues at the apical and interradicular regions of the LPS-affected DAJ (Figure 3). These significant shifts in effective strains within bone volumes when correlated with increasing joint space over time (Figure 2D) indicated that the changes in joint space alter load-induced deformation between the periodontal tissues. As such, the changes in bone structure, mechanical properties, and CF over time can collectively regulate the functional status of the DAJ albeit being pathological.

Chemo- and mechano-sensitive biochemical signals within the periodontal tissues and their interfaces are either opposed or augmented by metabolic stimuli/exogenous chemical cues. The significant changes in bone and PDL-space, specifically in the coronal regions (Figures 2B and 3), can be attributed to endotoxin-induced inflammatory signals from the vascularized bone and the

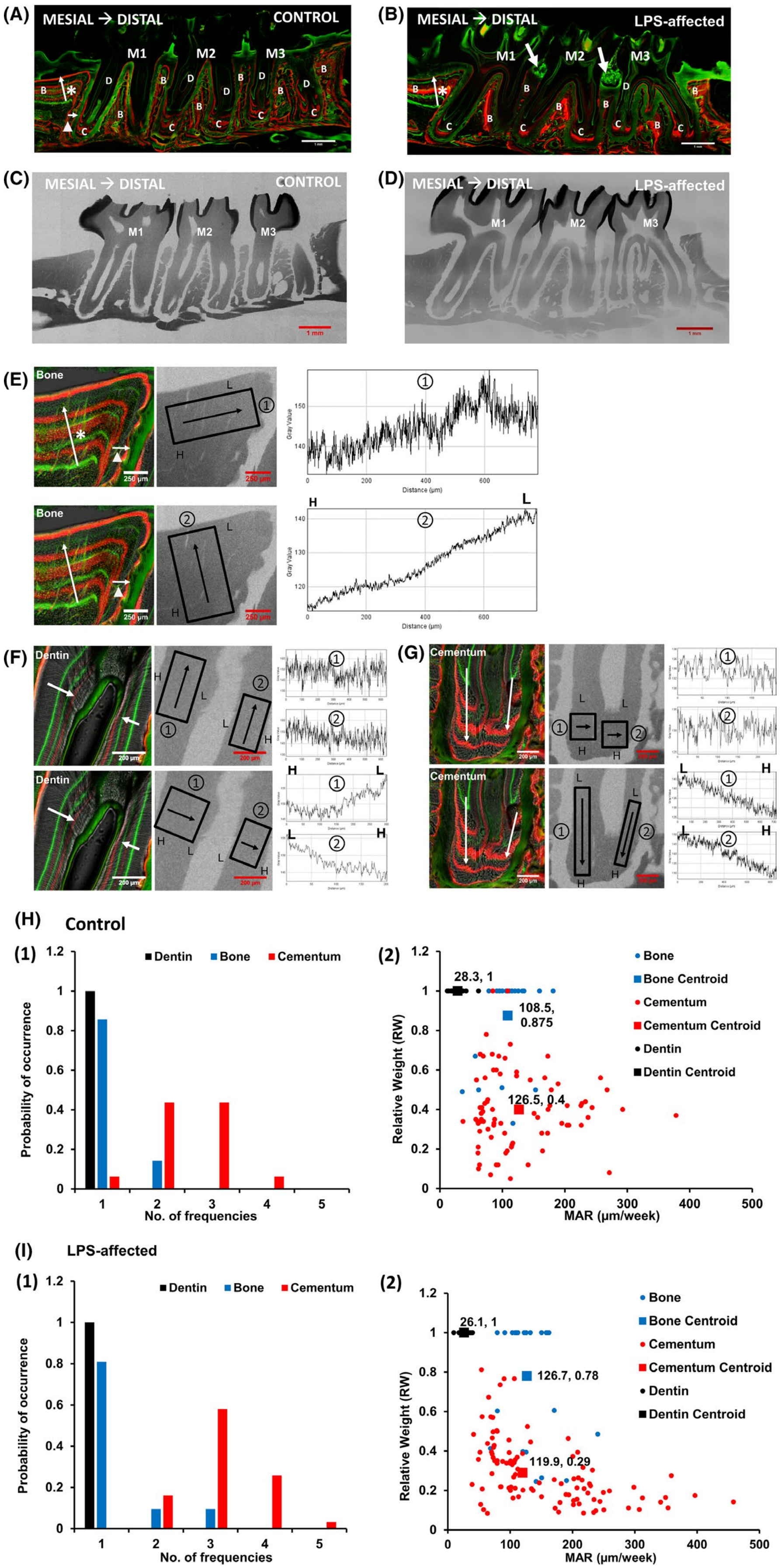

FIGURE 4 The orthogonality between mineral apposition layers (fluorochrome) and mineralizing front (radiograph) revealed nonlinear adaptation in cementum compared to linear adaptation in bone and dentin. (A-D) Fluorochrome (A, B) and X-ray (C, D) radiographs of control (A, C) and LPS-affected (B, D) hemi-maxillae are shown. (E) ROIs of LPS-affected bone in a fluorescent micrograph (left) and X-ray radiograph (right) are shown as line plots, and confirm significant mineral apposition in the coronal-apical (asterisk) compared to mesial-distal (triangle) direction. Note that in the LPS-affected group, only coronal-apical apposition is significantly visible through fluorochrome labeling. Similar patterns were observed in dentin (F) and cementum (G). (H, I) Probability and frequency of occurrences of bone, dentin, and cementum (1) are determined to further evaluate the relative weight (RW) of the respective mineral apposition rates (MAR) (2). Graphs illustrate individual MAR for bone, dentin, and cementum vs. their RW (linearity factor) and their centroids (squares) for (H, 2) control and (I, 2) LPS-affected conditions observed in any given final power spectrum of the ROI. See Figures A.2–5 and A.10 for more information

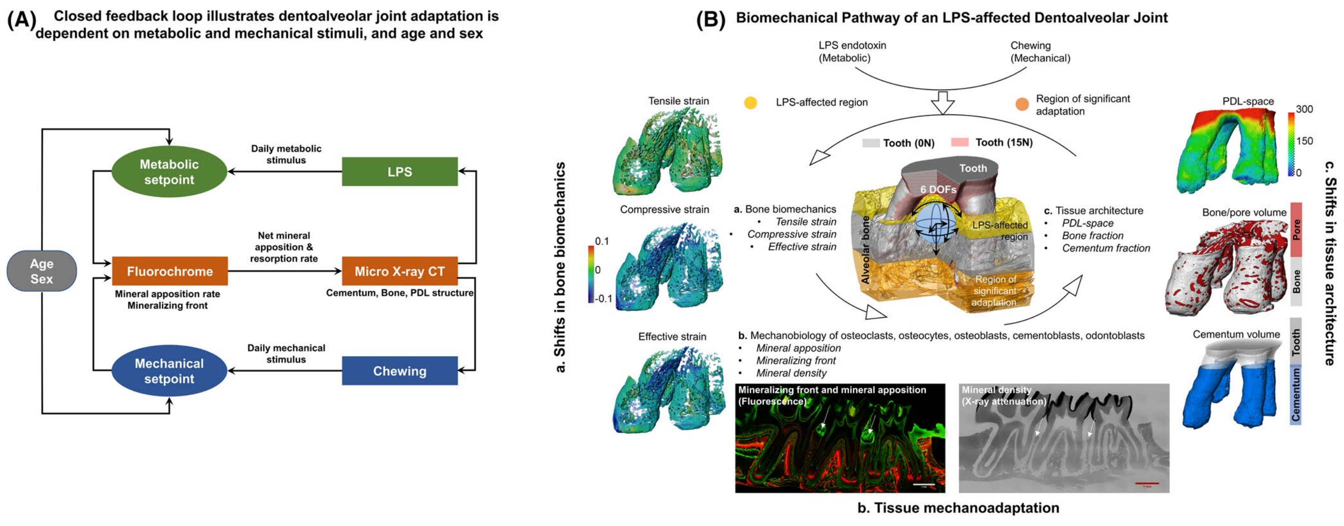

FIGURE 5 Closed feedback loop illustrates that DAJ adaptation is dependent on the daily metabolic and mechanical stimuli, all of which are dependent on age and sex of the rat. (A) The upper loop represents a metabolic response resulting from LPS endotoxin. The lower loop represents a mechanobiological response resulting from chewing load. Both metabolic and mechanical setpoints depend on and vary with age and sex. Fluorochrome technique was used to measure the mineral apposition rate, while micro-XCT imaging was performed to estimate tissue architecture. (B) The changes in tooth movement marked by changes in degrees of freedom (DOF) illicit changes in periodontal tissue biomechanics (a). These changes are marked as shifts in bone biomechanics/bone strain, resulting in tissue mechano-chemo adaptation (b). Sustained chewing in the presence of LPS (arrows) in rats illustrated a significant compensatory effect in periodontal tissues, namely cementum, despite observed changes in bone and dentin to a lesser extent. These fractional changes also were confirmed through fluorochrome labeling as increased nonlinear growth of cementum in apical location and linear growth of bone coronally and dentin laterally. (c) These shifts in tissue volume and architecture promote changes in PDL-space at the coronal, interradicular, and apical locations, and consequently changes in bone at the same locations and a nonlinear change in cementum fraction at the apical location. Sustained function perpetuates mechano-chemo adaptation and could coax the joint into pathological function (a net difference in DOFs compared to controls)

PDL (21). Shifts in PDL-space, BF, and CF (Figures 2 and 3) also result from age-specific biochemical signals within tissues and their resident cells (23) receiving only mechanical stimuli as observed in controls. The effect of metabolic/endotoxin stimuli on the periodontal complex, however, was revealed by correlating the spatiotemporal changes in joint space with changes in BF and CF (Figures 3Aa–C). The breakdown of the PDL in the acute phase (12), a gradual temporal decrease in BF, and a temporal increase in CF (Figures 3DF and 3F) hinted on the plausible effect of the LPS-stimulated adaptation.

Sustained chewing can potentiate the effect of endotoxin-induced inflammation (7). Chewing-induced mechanical strains within tissues transduce into tissue-specific cell responses (24) as elevated expressions of RANKL, TNF-alpha, and tartrate-resistant acid phosphatase (TRAP) during the first two weeks of LPS treatment (12,13). These observations were illustrated in our previous studies (12,13). In brief, the acute (first two weeks) biochemical shifts within tissues and PDL-entheses following LPS induction later (6 weeks and onwards) manifest into changes in DAJ functional biomechanics. The change in DAJ functional biomechanics, observed as changes in DOF of the tooth in the socket at 6 weeks, could result from resorption of bone and/or cementum and an increased PDL-space. These data bring to light the tipping of the metabolic balance between osteoblasts, osteoclasts, and osteocytes (25,26). As seen in various results, the mineral resorption-related acidic (TRAP) and the mineral formation-related alkaline (ALP) biochemical signals are localized at the vascularized and innervated ligament-bone and ligament-entheses of the periodontal complex (13). As such, the rate of movement of the resulting mineralizing front at these chemo- and mechano-sensitive entheses also were mapped as MAR in bone and cementum (Figure 4).

Based on the quantitative display of the fluorochrome micrographs, the observed coronal physical shifts in MAR of bone are comparable to the apical growth of cementum. Dentin illustrated limited tissue turnover compared to bone and cementum despite having similar organic and inorganic constituents (27). However, the nonlinear MAR observed in bone (RW < 1) and significantly in cementum (RW $<< 1$) indicated an "overdrive" metabolic activity in their respective resident cells. These data provide insights into the importance of the need for a synergistic fight between various cell types to maintain the PDL-space albeit under an "inflammatory attack" by endotoxins.

The temporal changes in BF and CF in LPS-affected DAJ could be potentiated by chewing-derived mechanical strains in the periodontal tissues (7). As such, we propose the extension of Hernandez's closed-loop feedback control system (28) applied to the skeletal bone to the alveolar bone. This control system that accounts for the effects of chemical and mechanical cues on mechano-chemo adaptation could help explain the compensatory growth of cementum in an LPS-affected DAJ (Figure 5).

5 | CONCLUSIONS and LIMITATIONS

The prolonged effect of LPS endotoxin (12 weeks) on the periodontal complex of rodents in this study could have developed a "tolerance to LPS endotoxin" (14) analogous to "tolerance to antibiotics." Previous studies from our laboratory, however, have immunolocalized TNF-alpha and TRAP at site-specific locations of the periodontal complex (12,13,29). For this reason, the observed presence of cytokines and proinflammatory enzymes, and changes in PDL-collagen birefringence and orientation should be confirmed by mapping the spatiotemporal expressions of proinflammatory markers using RT-PCR and spatial transcriptomics-related experiments.

This study illustrated if the sustained local presence of LPS endotoxin by using a ligature can change both the periodontal tissue and DAJ function. It is important to note that the increased tooth movement resulting from LPS endotoxin within the socket compromises DAJ functional status. The multiscale imaging and biomechanical analyses provided a comprehensive outlook on the functional status of a DAJ. Contextualization of tissue-specific local effects indicated that adaptations were not limited to the site of insult but extended into biomechanically active regions farther away from the site of insult. Local mineral resorption (clastic) activity is accompanied and balanced by an overall formation (blastic) event, which is not limited to bone but also extends into cementum. Further investigation of cementum adaptation as a plausible built-in compensatory mechanism to reestablish functional competence of an LPS-affected DAJ is warranted.

ACKNOWLEDGMENTS

The authors thank the Biomaterials and Bioengineering Correlative Microscopy Core (http://bbcmc.ucsf.edu), UCSF for the use of their MicroXCT-200. The authors declare no potential conflicts of interest with respect to the authorship and/or publication of this article. Funding: This work was supported by the National institutes of Health, NIDCR R01 DE022032 (SPH) and NIDCR R21 DE027138 (SPH).

DATA AVAILABILITY STATEMENT

The data that support the findings of this study are available from the corresponding author upon reasonable request.

ORCID

Bo Wang https://orcid.org/0000-0002-2249-8896
Putu Ustriyana https://orcid.org/0000-0001-9804-3081
Sunita. P. Ho https://orcid.org/0000-0001-9999-8226

REFERENCES

1. Beertsen W, McCulloch CA, Sodek J. The periodontal ligament: a unique, multifunctional connective tissue. *Periodontol 2000*. 1997;13(1):20–40.
2. Herring SW. Biomechanics of teeth in bone: function, movement, and prosthetic rehabilitation. *Mineralized Tissues in Oral and Craniofacial Sceince Biological Principles and Clincal Correlates*. 2012;1:255.
3. Nanci A, Bosshardt DD. Structure of periodontal tissues in health and disease. *Periodontol 2000*;2006(40):11-28.
4. Giannobile WV, Lynch SE, Denmark RG, Paquette DW, Fiorellini JP, Williams RC. Crevicular fluid osteocalcin and pyridinoline cross-linked carboxyterminal telopeptide of type I collagen (ICTP) as markers of rapid bone turnover in periodontitis. A pilot study in beagle dogs. *J Clin Periodontol*. 1995;22:903-910.
5. Buduneli N, Kinane DF. Host-derived diagnostic markers related to soft tissue destruction and bone degradation in periodontitis. *J Clin Periodontol*. 2011;38(11):85-105.
6. Hausmann E, Dunford R, Christersson L, Allen K, Wokesjo U. Crestal alveolar bone change in patients with periodontitis as observed by subtraction radiography: an overview. *Adv Dent Res*. 1988;2:378-381.
7. Oh S, Chung H, Chang S, Lee SH, Seok SH, Lee H. Effect of Mechanical Stretch on the DNCB-induced Proinflammatory Cytokine Secretion in Human Keratinocytes. *Sci Rep*. 2019;9:5156.
8. Nanci A. *Ten Cate's Oral Histology*: Elsevier, 2017.
9. Raetz CR, Whitfield C. Lipopolysaccharide endotoxins. *Annu Rev Biochem*. 2002;71:635-700.
10. Raetz CR. Biochemistry of endotoxins. *Annu Rev Biochem*. 1990;59:129-170.
11. Jang AT, Merkle A, Fahey K, Gansky SA, Ho SP. Multiscale biomechanical responses of adapted bone-periodontal ligament-tooth fibrous joints. *Bone*. 2015.
12. Lee JH, Lin JD, Fong JI, Ryder MI, Ho SP. The adaptive nature of the bone-periodontal ligament-cementum complex in a ligature-induced periodontitis rat model. *Biomed Res Int*. 2013;2013:1–17.
13. Lin JD, Lee J, Ozcoban H, Schneider GA, Ho SP. Biomechanical adaptation of the bone-periodontal ligament (PDL)-tooth fibrous joint as a consequence of disease. *J Biomech*. 2014;47:2102-2114.
14. Graves DT, Kang J, Andriankaja O, Wada K, Rossa C Jr. Animal models to study host-bacteria interactions involved in periodontitis. *Front Oral Biol*. 2012;15:117-132.
15. Bosshardt D, Luder HU, Schroeder HE. Rate and growth pattern of cementum apposition as compared to dentine and root formation in a fluorochrome-labelled monkey (Macaca fascicularis). *J Biol Buccale*. 1989;17:3-13.
16. Garetto LP, Chen J, Parr JA, Roberts WE. Remodeling dynamics of bone supporting rigidly fixed titanium implants: a histomorphometric comparison in four species including humans. *Implant Dent*. 1995;4:235-243.
17. Herber RP, Fong J, Lucas SA, Ho SP. Imaging an adapted dentoalveolar complex. *Anatomy Res Inter*. 2012;2012:1–13.
18. Du J, Lee JH, Jang AT, et al. Biomechanics and strain mapping in bone as related to immediately-loaded dental implants. *J Biomech*. 2015;48:3486-3494.
19. Jang A, Prevost R, Ho SP. Strain mapping and correlative microscopy of the alveolar bone in a bone–periodontal ligament–tooth fibrous joint. *Proc Inst Mech Eng [H]*. 2016;230(9):847–857.
20. Wang B, Kim K, Srirangapatanam S, et al. Mechanoadaptive strain and functional osseointegration of dental implants in rats. *Bone*. 2020;115375.
21. Daly CG, Seymour GJ, Kieser JB. Bacterial endotoxin: a role in chronic inflammatory periodontal disease? *J Oral Pathol*. 1980;9:1-15.
22. Snyderman R. Role for endotoxin and complement in periodontal tissue destruction. *J Dent Res*. 1972;51:356-361.
23. Leong NL, Hurng JM, Djomehri SI, Gansky SA, Ryder MI, Ho SP. Age-related adaptation of bone-PDL-tooth complex: Rattus-Norvegicus as a model system. *PLoS One*. 2012;7:e35980.
24. Ingber DE. Tensegrity: the architectural basis of cellular mechanotransduction. *Annu Rev Physiol*. 1997;59:575-599.
25. Robling AG, Turner CH. Mechanical signaling for bone modeling and remodeling. *Crit Rev Eukaryot Gene Expr*. 2009;19:319-338.

26. Dieterle MP, Husari A, Steinberg T, Wang X, Ramminger I, Tomakidi P. Role of Mechanotransduction in Periodontal Homeostasis and Disease. *J Dent Res*. 2021;220345211007855.
27. Opsahl Vital S, Gaucher C, Bardet C, et al. Tooth dentin defects reflect genetic disorders affecting bone mineralization. *Bone*. 2012;50:989-997.
28. Hernandez CJ, Beaupre GS, Carter DR. A model of mechanobiologic and metabolic influences on bone adaptation. *J Rehabil Res Dev*. 2000;37:235-244.
29. Lee JH, Pryce BA, Schweitzer R, Ryder MI, Ho SP. Differentiating zones at periodontal ligament-bone and periodontal ligament-cementum entheses. *J Periodontal Res*. 2015;50:870-880.

SUPPORTING INFORMATION

Additional supporting information may be found in the online version of the article at the publisher's website.

How to cite this article: Wang B, Ustriyana P, Tam CS, et al. Functional Adaptation of LPS-affected Dentoalveolar Fibrous Joints in Rats. *J Periodont Res*. 2021;00:1–11. https://doi.org/10.1111/jre.12946